Available online at www.sciencedirect.com

SCIENCE DIRECT

Remote Sensing of Environment 96 (2005) 228 – 245

Remote Sensing of Environment

www.elsevier.com/locate/rse

Spatial and temporal patterns of remotely-sensed and field-measured rainfall in southern California

Nikolay P. Nezlin*, Eric D. Stein

Southern California Coastal Water Research Project, Westminster, CA 92683-5218, USA

Received 16 June 2004; received in revised form 23 February 2005; accepted 26 February 2005

Abstract

Quantification of spatial and temporal patterns of rainfall is an important step toward developing regional hydrological models. However, traditionally used rain gauge data are sparse and do not always provide adequate spatial representation of rainfall. In this study, we evaluated the daily 1-degree resolution remotely-sensed atmospheric precipitation data provided by Global Precipitation Climatology Project (GPCP) as an alternative to rain gauge-measured data. We analyzed data from the watersheds of southern California during the period of 1996–2003, focusing on the comparison of patterns of spatial, seasonal, and interannual rainfall dynamics. We used Empirical Orthogonal Functions to discern the patterns of precipitation and atmospheric circulation at different time scales, from synoptic to interannual. The correlation between the daily rain gauge-measured and remotely-sensed precipitation was poor and the resulting patterns of remotely-sensed precipitation are different than the temporal patterns of precipitation accumulated by rain gauges. These differences likely result from the fact that the precipitable water concentration measured by satellites is not always highly correlated to rainfall reaching the earth surface. Differences in the spatial resolution and coverage of the two methods and the differential influence of orographic effects and wind patterns on each also contribute to low correlations. We conclude that daily remotely-sensed precipitation produced at GPCP is not currently appropriate for use in assessing fine-scale hydrological processes in arid zones like southern California, and would not be a recommended surrogate for event-based hydrologic modeling. At the same time, the interannual variabilities of remotely-sensed and gauge-measured precipitation were highly correlated and the regional patterns of gauge-measured and remotely-sensed precipitation variability were similar; though the total precipitation estimated from satellite data was substantially lower than the gauge-measured data. Therefore, remotely-sensed precipitation data may be appropriate for use in long-term regional hydrologic or climate modeling focused on trends and patterns of rainfall in southern California. Both data sets showed that precipitation generally decreases from the northern to the southern watersheds. At interannual time-scale, the rainfall is related to the ENSO cycle. At synoptic time-scales, the rainfall patterns in southern California result from atmospheric moisture transport from the south–southwest.

Keywords: Precipitation; Wind; ENSO; Southern California; 32–35° N; 121–116° W

1. Introduction

During recent years, the increased accuracy and availability of remotely-sensed data has made it an alternative to traditional rain gauge data for developing regional models of rainfall, runoff, and river plume dynamics. The observations of atmospheric precipitation collected by satellites play a critical role in the monitoring of meteorological processes over the majority of the Earth's surface (Arkin & Ardanuy, 1989; Huffman et al., 2001). The advantage of remotely-sensed data over rain gauges is that they provide relatively uniform and consistent spatial and temporal coverage of rainfall information. Rain gauges may be less common, less densely deployed, or less consistently maintained in the open ocean and in unpopulated areas, resulting in spatial and temporal data gaps. Daily digital satellite observations of rainfall have only been widely available for the past few years, and their

* Corresponding author. Tel.: +1 714 372 9227.
E-mail address: nikolayn@sccwrp.org (N.P. Nezlin).

0034-4257/$ - see front matter © 2005 Elsevier Inc. All rights reserved.
doi:10.1016/j.rse.2005.02.005

accuracy and application for rainfall–runoff analysis has not been statistically evaluated. Nevertheless, the remotely-sensed monitoring of the environment is developing rapidly and a sufficient duration of data is now available for more rigorous evaluation.

Southern California has an arid Mediterranean climate with short rainstorm events, which typically occur during the winter season. The rainstorm patterns are affected by a complex combination of atmospheric circulation and topographic effects. Low-pressure winter storms typically move southward from the North Pacific along the western edge of North America. As these storm systems approach southern California, they are moderated by the Pacific high-pressure system and a thermal low to the east, which deflects many storms (Bailey, 1966). As a result, the average annual rainfall in southern California is only 30–50 cm. During winter, the center of high pressure moves to a southwest position, allowing brief, intense Pacific storm fronts to penetrate the area (Lu et al., 2003). Rainfall patterns are further moderated by a temperature inversion created by the ring of mountain ranges that define southern California. The east–west Transverse Ranges and the north–south Peninsular Ranges create a "coastal basin" where cool, dense air is trapped, often deflecting marine winds over the area, resulting in much weaker wind patterns than over the open ocean and lower rainfall than areas to the east (Dorman & Winant, 1995). In addition to annual and seasonal atmospheric cycles, rainfall patterns are governed by atmospheric processes that operate at interannual to multi-decadal time scales, such as the El Niño Southern Oscillation (ENSO) and the Pacific Decadal Oscillation (PDO).

Understanding the variability of rainfall patterns is an important element to developing conceptual and predictive models of runoff, pollutant loading, and river plume dynamics. For example, the intensity and spatial distribution of rainfall can affect the magnitude and duration of pollutant washoff to the ocean (Tiefenthaler & Schiff, 2003; Vaze & Chiew, 2003). The interval between rain events, along with the characteristics of the watershed, will influence the lag time between rainfall and runoff and the portion of total precipitation that translates to surface runoff (Ackerman et al., 2005; Mount, 1995; Ward & Elliot, 1995). Remotely-sensed data offers the potential to monitor and analyze patterns and processes that control rainfall variability, which are critical to the accuracy of models used to support the development and evaluation of storm water management practices.

In this study, we compare the spatio-temporal rainfall patterns derived from the analysis of remotely-sensed and gauge-measured precipitation in southern California. The remotely-sensed measurements of atmospheric precipitation are based on the estimation of the concentration of precipitable water vapor in the atmosphere rather than rainfall reaching the earth surface. Therefore, the correlation between the remotely-sensed and gauge-measured data may not be high. The goal of this study is to answer the question: how well does modern remotely-sensed atmospheric precipitation measurements represent the basic features of rainfall in the study area, i.e., how confident would we be using these data in predictive hydrological models that relate runoff, pollutant loading, and plume dynamics to climatic cycles at various spatial and temporal scales? We focus our analysis on precipitation over the southern California nearshore zone and the twelve main coastal watersheds that are the relevant functional units for freshwater discharge to the Southern California Bight (Ackerman & Schiff, 2003; Ackerman & Weisberg, 2003; Ackerman et al., 2005). We compare daily digital satellite precipitation data to precipitation measured by standard rain gauge stations and use statistical methods to quantify spatial and temporal patterns in rainfall and wind. We then compare these patterns to global climatological cycles (e.g. ENSO and PDO) to discern the effect of forcing functions operating at different time scales on regional precipitation patterns.

2. Methods

2.1. Precipitation data

Satellite and rain gauge rainfall data were collected for the period 1996–2003, during which time daily satellite images for rainfall are readily available. Daily digital maps of remotely-sensed precipitation of one-degree resolution (1DD), produced as a part of the Global Precipitation. Climatology Project (GPCP), were obtained from the NASA Goddard Space Flight Center Distributed Active Archive Center (NASA GSFC DAAC). GPCC data were collected by four types of satellite sensors: (1) geo-synchronous (geostationary) satellites with infrared sensors (geo-IR), including Geosynchronous Operational Environmental Satellites (GOES, USA), Geosynchronous Meteorological Satellite (GMS, Japan), and Meteorological Satellite (METEOSAT, European Community); (2) National Oceanic and Atmospheric Administration (NOAA) series polar-orbiting low-earth-orbit satellites with infrared sensors (leo-IR); (3) Special Sensor Microwave/Imager (SSM/I) multi-channel passive microwave radiometers on Defense Meteorological Satellite Program (DMSP) satellites; and (4) Television and Infrared Observation Satellite (TIROS) Operational Vertical Sounder (TOVS) data derived from analysis of the information collected by High-Resolution Infrared Sounder 2 (HIRS2) and Microwave Sounding Unit (MSU) aboard the NOAA series of polar-orbiting operational meteorological satellites. The monthly GPCP "satellite-gauge precipitation product" (SG) was used for calibration of 1DD data. The results of "merged" processing of geo-IR, leo-IR, and SSM/I data provided remotely-sensed precipitation estimates in the zone 40° N–40° S. TOVS data, which

covered the zone outside this latitude band, were not used in this study. The details of the algorithm of processing and validation of 1DD GPCP data are described in (Huffman et al., 2001). The format of GPCP 1DD data is a daily global grid of 1° spatial resolution. We extracted for analysis the data from four 1° by 1° grid cells covering the area located between 32° and 35° N, and 120° and 116° W (Fig. 1).

Daily rain gauge data were obtained from 98 meteorological stations located in southern California (Fig. 1). The data were downloaded from the NOAA National Data Center Climate Data Online (NNDC/CDO) Internet site. Each observation represents precipitation during a 24-h period preceding the observation time. The precise time of observation differed between stations during different periods; therefore, we attributed each observation to an entire day and did not analyze the variability at a time-scale less than daily. Not all stations had continuous data for the entire 7.5-year period of analysis. To obtain continuous time-series of precipitation in different parts of the study area, all stations were classified to 12 watersheds (Appendix A) and the precipitation was averaged over each watershed area.

2.2. Wind data

Wind data were obtained from the National Center for Environmental Prediction (NCEP); the global wind data are supplied by the NASA GSFC DAAC as ancillary information for SeaWiFS users. These files contain regular grids of zonal and meridional wind speeds at 10 m above the earth surface interpolated on an equidistant cylindrical projection of 1° spatial resolution and 6-h temporal resolution (12-h during some periods in 1998 and 1999). Wind pattern was analyzed within the rectangle from 31° to 36° N and from 122° to 115° W during the period from March 1997 to October 2003.

2.3. Statistical analysis

Seasonal patterns were estimated by averaging precipitation over the entire 7.5 years of observations (January 1996–June 2003) for each watershed during each day of the seasonal cycle. We used the Empirical Orthogonal Functions (EOF) method to analyze spatio-temporal variability of precipitation and wind and the relationship between the two. This statistical approach is a convenient method for analysis of the successive patterns of spatially distributed data. The EOF method (Priesendorfer, 1988) decomposes space- and time-distributed data into a set of orthogonal functions (spatial maps) and the corresponding principle components (time series). Each of these orthogonal functions is then ranked by its variance. In this study, we analyze total values of precipitation and wind rather than their anomalies; therefore, we did not analyze pure spatial or temporal variance, but the joint space-time

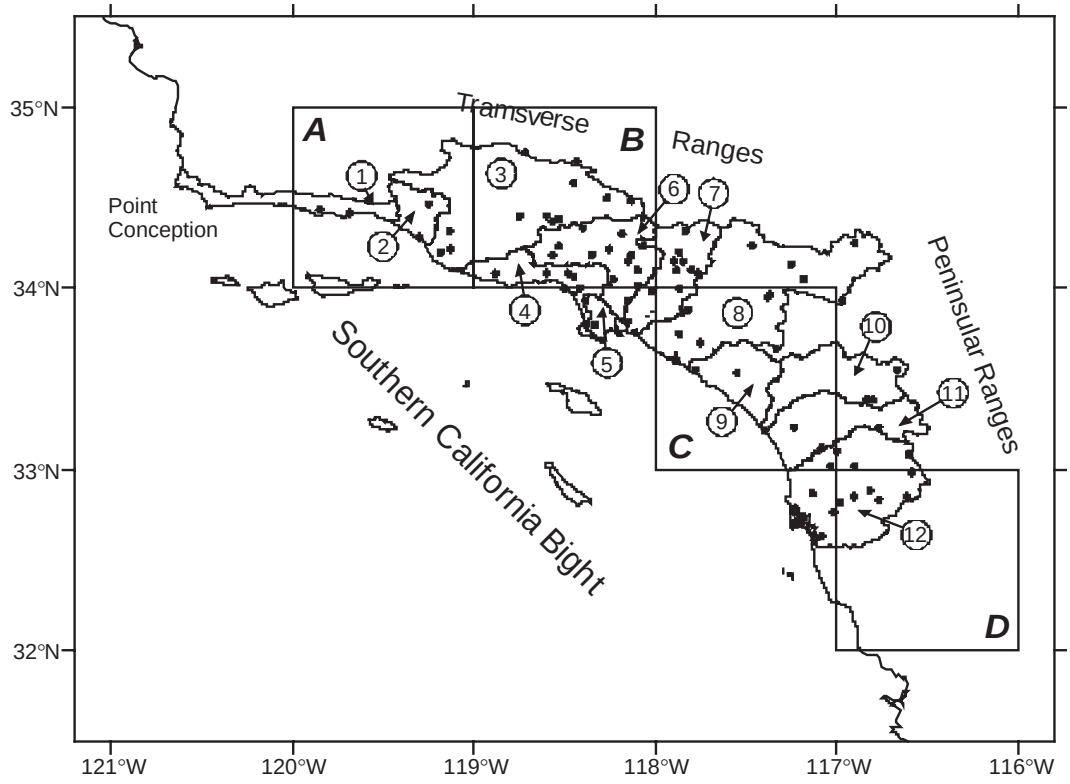

Fig. 1. The map of watersheds (1–12, see Table 1) and rain gauge stations (solid circles) in southern California; the location of grid cells of the remotely-sensed precipitation (GPCP): 34°30′ N, 119°30′ W (A); 34°30′ N, 118°30′ W (B); 33°30′ N, 117°30′ W (C); 32°30′ N, 116°30′ W (D).

Table 1
Correlation between the variations of precipitation in the watersheds of southern California and the remotely-sensed precipitation in four 1° × 1° grid cells during October 1996–June 2003

		34°30′ N, 119°30′ W	34°30′ N, 118°30′ W	33°30′ N, 117°30′ W	32°30′ N, 116°30′ W
1	Santa Barbara Creek	+0.47 (+0.54)	+0.39 (+0.49)	+0.27 (+0.34)	+0.17 (+0.23)
2	Ventura River	+0.44 (+0.46)	+0.48 (+0.53)	+0.41 (+0.44)	+0.25 (+0.31)
3	Santa Clara River	+0.52 (+0.63)	+0.48 (+0.62)	+0.41 (+0.51)	+0.30 (+0.41)
4	Santa Monica Bay	+0.46 (+0.57)	+0.45 (+0.57)	+0.39 (+0.48)	+0.30 (+0.39)
5	Dominguez Channel	+0.58 (+0.67)	+0.55 (+0.66)	+0.50 (+0.58)	+0.38 (+0.47)
6	Los Angeles River	+0.46 (+0.57)	+0.46 (+0.59)	+0.42 (+0.51)	+0.33 (+0.41)
7	San Gabriel River	+0.45 (+0.51)	+0.42 (+0.53)	+0.39 (+0.47)	+0.27 (+0.35)
8	Santa Ana River	+0.41 (+0.51)	+0.46 (+0.57)	+0.41 (+0.49)	+0.26 (+0.36)
9	San Juan Creek	+0.42 (+0.50)	+0.48 (+0.55)	+0.43 (+0.47)	+0.25 (+0.32)
10	Santa Margarita River	+0.32 (+0.41)	+0.37 (+0.48)	+0.33 (+0.39)	+0.26 (+0.32)
11	San Luis Rey River/Escondido Creek	+0.27 (+0.41)	+0.31 (+0.45)	+0.30 (+0.38)	+0.24 (+0.32)
12	San Diego River	+0.37 (+0.49)	+0.41 (+0.55)	+0.38 (+0.48)	+0.32 (+0.41)

In parentheses correlation coefficients estimated from the seasonal patterns of precipitation (365 averaged climatic days).

variance. The EOF method was applied to remotely-sensed precipitation (2464 daily observations during October 1st 1996–June 30th 2003 at each of 35 grid cells of the rectangle 31.5–35.5° N; 121.5–115.5° W), gauge-measured precipitation (2738 daily observations during January 1st 1996–June 30th 2003 at each of 12 watersheds), and wind (8985 observations during March 13th 1997–June 30th 2003 at each of 48 grid cells of the rectangle 31–36° N; 122–115° W; zonal and meridional wind components in each cell resulted in total 96 variables).

To relate the long-scale meteorological variations in southern California to the global climatic meteorological cycles, we used the NINO3 index (sea surface temperature anomalies averaged over the region 5° S–5° N; 150–90° W in equatorial Pacific) and the Southern Oscillation Index (SOI, the difference between the standardized measurements of the Sea Level Atmospheric Pressure in Tahiti and Darwin) obtained from the International Research Institute of Climate Prediction (Columbia University, USA).

3. Results

3.1. Spatial patterns of rainfall

The daily rainfall data measured by the two methods was not highly correlated. Correlation analysis revealed that daily remotely-sensed precipitation data was only moderately comparable to rain gauge data, with correlations being stronger in the northern watersheds than in the southern watersheds (Table 1). Correlation coefficients between precipitation in each watershed and in the four grid cells of the global remotely-sensed precipitation map ranged from +0.17 to +0.67. Correlations were stronger based on seasonal variations (i.e., 365 averaged climatic days) than on the basis of the entire period of observations (October 1996–June 2003). However, spatial relationships between the remotely-sensed grids and the associated watersheds were weak. Correlation coefficients between a specific 1° by 1° grid cell and its corresponding watersheds were only slightly higher than with the other watersheds in the region. This is especially true for the cell that overlies the southern watersheds (Location D at Fig. 1), where low correlation coefficients were comparable with all 12 watersheds. The low correlation can be attributed partly to the fact that this cell is spatially offset from the southern watersheds (see Fig. 1). To verify this conclusion, we rebinned the rain gauge stations according to the boundaries of four GPCP grid cells rather than twelve watersheds (Table 2). This offered a more direct spatial comparison of the remotely-sensed and rain gage data. Nevertheless, the resulting correlation coefficients between the two approaches did not improve and were similar to those shown in Table 1.

In contrast to the results from the analysis of daily rainfall data, both remotely-sensed and rain gauge data revealed similar regional annual rainfall patterns of decreasing precipitation from northern to southern watersheds (Tables 3 and 4). Maximum mean annual rain gauge-measured precipitation (54.8 cm/year) was observed in the northernmost Santa Barbara Creek watershed and the minimum mean annual precipitation (32.54 cm/year)

Table 2
Correlation between the variations of remotely-sensed and gauge-measured precipitation in four 1° × 1° grid cells during October 1996–June 2003

	34°30′ N, 119°30′ W	34°30′ N, 118°30′ W	33°30′ N, 117°30′ W	32°30′ N, 116°30′ W
34°30′ N, 119°30′ W	+0.50 (+0.57)	+0.45 (+0.53)	+0.34 (+0.41)	+0.23 (+0.29)
34°30′ N, 118°30′ W	+0.49 (+0.61)	+0.48 (+0.61)	+0.43 (+0.53)	+0.33 (+0.44)
33°30′ N, 117°30′ W	+0.44 (+0.55)	+0.50 (+0.61)	+0.45 (+0.53)	+0.31 (+0.41)
32°30′ N, 116°30′ W	+0.21 (+0.32)	+0.26 (+0.39)	+0.25 (+0.35)	+0.21 (+0.32)

Table 3
Summary of rain gauge data for twelve watersheds in southern California that discharge to the Pacific Ocean

#	Watershed	Area (km^2)	Annual rain gauge-measured precipitation in 1996–2003 (cm)			
			Mean	Minimum (2001/2002)	Maximum (1997/1998)	Max/Min
1	Santa Barbara Creek	971	54.80	23.19	119.35	5.1
2	Ventura River	696	47.33	19.19	108.66	5.7
3	Santa Clara River	5164	37.34	14.82	83.73	5.6
4	Santa Monica Bay	1170	39.46	11.59	84.86	7.3
5	Dominguez Channel	300	33.92	11.01	79.88	7.2
6	Los Angeles River	2161	48.04	16.83	108.79	6.5
7	San Gabriel River	1758	43.25	9.44	101.19	10.7
8	Santa Ana River	5101	33.85	10.68	78.93	7.4
9	San Juan Creek	1284	36.88	12.45	89.31	7.2
10	Santa Margarita River	1915	36.98	14.88	80.56	5.4
11	San Luis Rey River/Escondido Creek	2002	38.47	14.92	96.69	6.5
12	San Diego River	3561	32.54	12.34	77.58	6.3

Watersheds are listed from north to south.

occurred in the southernmost San Diego River watershed. The same north to south trend was apparent in the annual remotely-sensed precipitation data (Fig. 2 and Table 4), although the absolute values were substantially lower, from 28.4 cm/year in the north to 11.3 cm/year in the south.

Year-to-year variability of both remotely-sensed and gauge-measured precipitation was very high, as is typical for Mediterranean climates (see Tables 3 and 4). In all cases, the maximum precipitation was observed in 1997/1998 and the minimum was in 2001/2002. In gauge-measured precipitation, the ratio between the "wettest" and the "driest" years ranged from 5.1-fold for the Santa Barbara Creek Watershed to 10.7-fold for the San Gabriel River Watershed (Table 3). In remotely-sensed precipitation, the ratio ranged from 4.9 for the northernmost watershed to 7.0 for the southernmost one (Table 4). However, no clear north to south pattern was observed in relative differences between wet and dry years in the gauge-measured data.

The seasonal patterns of gauge-measured (Fig. 3) and remotely-sensed (Fig. 4) precipitation were similar. In gauge-measured data, seasonal patterns were consistent among watersheds, but the magnitude of difference between the wet and dry portions of the year generally decreased from north to south, i.e., seasonal patterns were muted in the southern watersheds (Fig. 3). Rainstorms generally occurred from the end of October to April of the next year, with most intensive rainstorms in February. Northern watersheds regularly experienced daily mean rain gauge precipitation in excess of 2 cm, whereas in the southern watersheds it rarely exceeded 1 cm. As with the total annual precipitation, the remotely-sensed data exhibited a similar pattern, but daily mean values were generally lower than those observed in the rain gauges (Fig. 4).

The spatio-temporal patterns revealed by the Empirical Orthogonal Functions were similar in remotely-sensed and gauge-measured precipitation. Results of the EOF analysis identified the modes that contributed to spatial variability in precipitation patterns, with the first two modes accounting for 84.17% and 70.56% of the total variability in both the rain gauge and remotely-sensed data, respectively (Table 5).

The first EOF modes for both data sets represented total rainstorm magnitude. In the rain gauge data, the first EOF mode accounted for 71.36% of the total variability between the 12 watersheds analyzed. Factor loadings for the first EOF mode for all 12 watersheds were positive and high, ranging from +0.66 to +0.94 (Table 6). In general, the watersheds located in the center of the study area provided maximum contribution to the total variability. For the remotely-sensed precipitation data, the first EOF mode explained 58.88% of variability and its maximum was also located in the center of the study area (Table 5, Fig. 5A). The second EOF modes for both data sets represented the north/south variability of rainstorms over southern Cal-

Table 4
Annual remotely-sensed precipitation (cm) in four 1° × 1° grid cells (see Fig. 1)

#	Center of the 1° × 1° grid cell	Annual remotely-sensed precipitation in 1996–2003 (cm)			
		Mean	Minimum (2001/2002)	Maximum (1997/1998)	Max/min
1	34°30′ N, 119°30′ W	28.44	12.52	61.62	4.9
2	34°30′ N, 118°30′ W	24.13	9.12	51.83	5.7
3	33°30′ N, 117°30′ W	16.54	5.47	37.33	6.8
4	32°30′ N, 116°30′ W	11.31	3.69	25.87	7.0

Grid cells are listed from north to south.

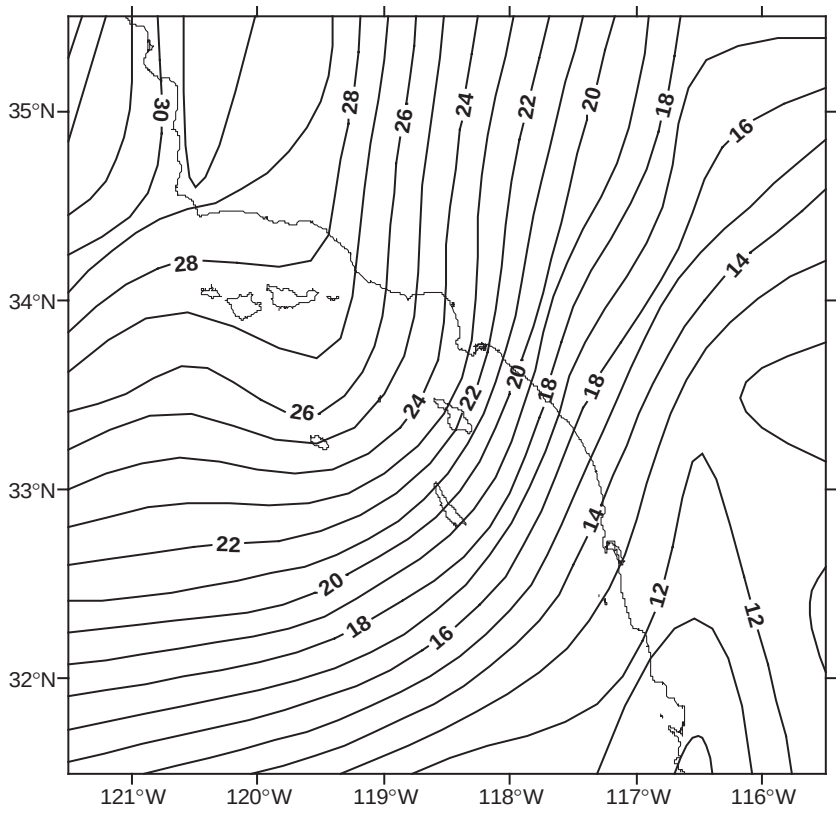

Fig. 2. Precipitation contours (cm/year) based on remotely-sensed data (GPCP) averaged over the period of October 1996–June 2003.

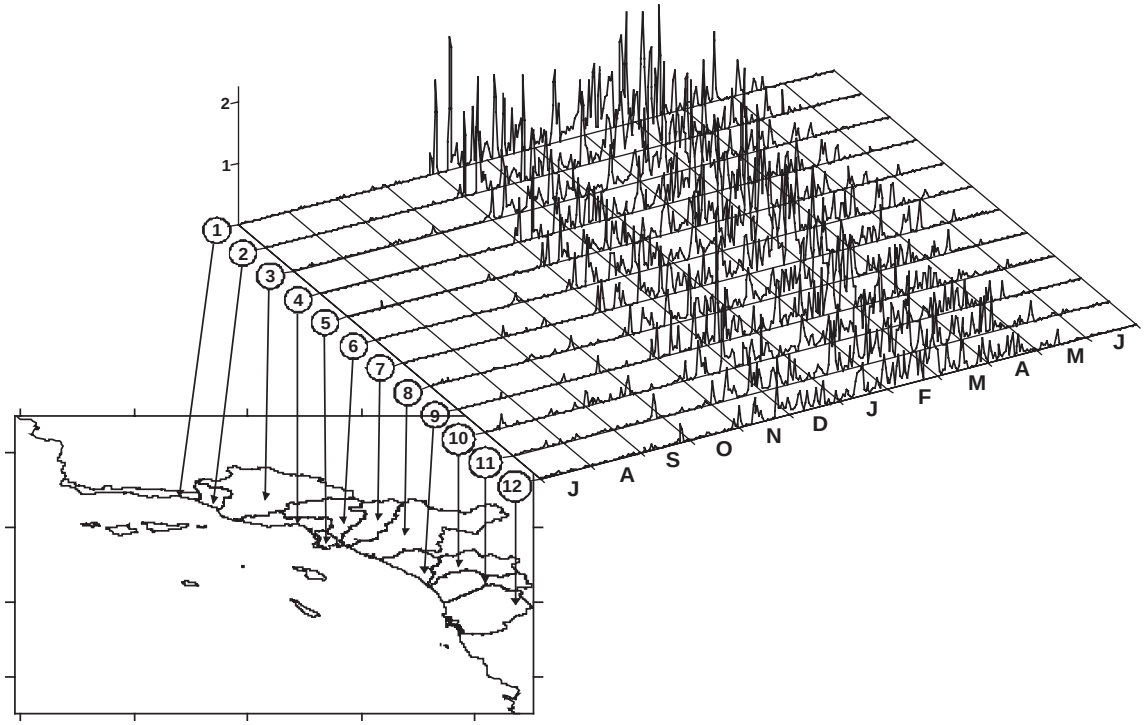

Fig. 3. Seasonal patterns of rain gauge-measured precipitation over different watersheds in southern California. *X*-axis represents months from July to June; numbers in circles along *Y*-axis indicate watersheds (Table 1); *Z*-axis represents mean daily precipitation (cm).

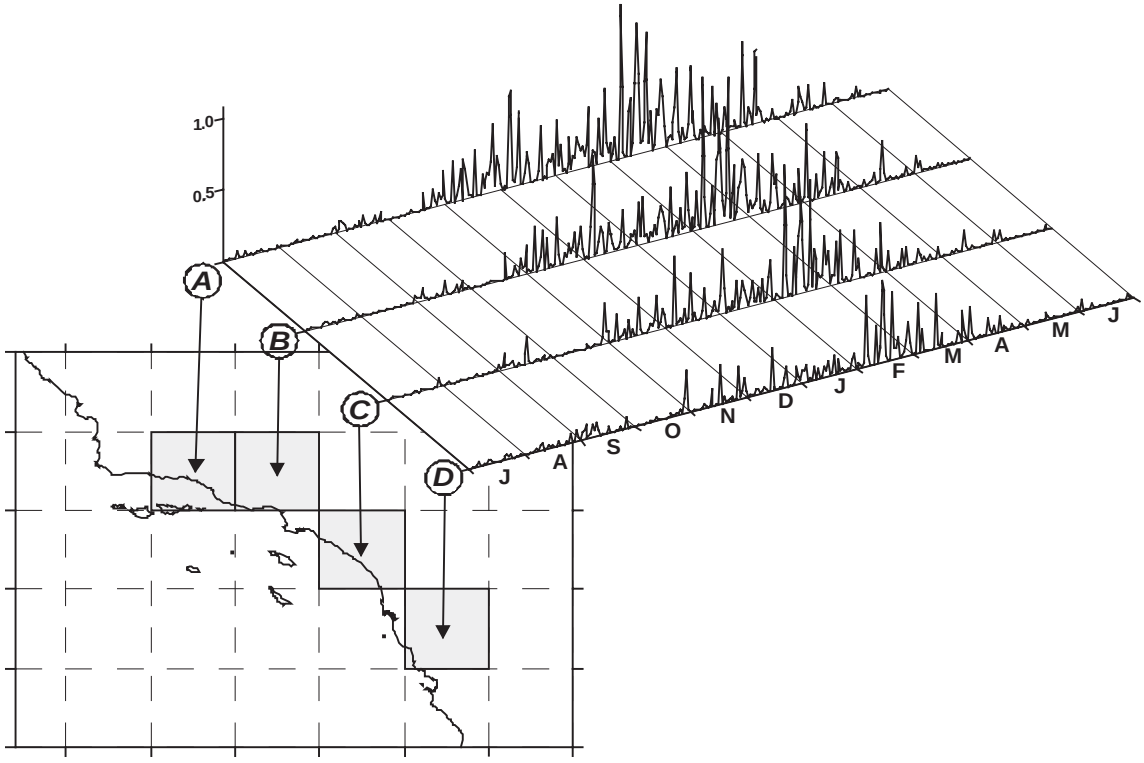

Fig. 4. Seasonal patterns of remotely-sensed precipitation in four 1° × 1° grid cells over southern California: 34°30′ N, 119°30′ W (A); 34°30′ N, 118°30′ W (B); 33°30′ N, 117°30′ W (C); 32°30′ N, 116°30′W (D). *X*-axis represents months from July to June; *Z*-axis represents mean daily precipitation (cm).

ifornia (Table 5, Fig. 5B); the second EOF mode explained 12.81% of the total variability of rain gauge precipitation and 11.68% of the total variability of the remotely-sensed precipitation. The north-to-south gradient of the second EOF modes indicated that a positive change of these modes was related to a migration of the center of a rainstorm to the south. The third EOF modes of both data sets explained only 4.25% and 6.86% of total variability and did not exhibit a clear pattern of spatio-temporal variations; therefore, they were not analyzed further.

3.2. Relationship between rain and wind patterns

To compare the spatio-temporal patterns of precipitation derived from remotely-sensed and gauge-measured observations, we analyzed the correlation between their dynamics and the patterns of wind variability in southern California.

Table 5
The percentage of total variance of precipitation and wind explained by first three EOF modes

Mode	Percent of variance (%)		
	Precipitation in rain gauges	Remotely-sensed precipitation	Wind
1	71.36 (71.36)	58.88 (58.88)	32.78 (32.78)
2	12.81 (84.17)	11.68 (70.56)	19.56 (52.34)
3	4.25 (88.42)	6.86 (77.42)	8.17 (60.51)

In parenthesis cumulative percentage of total variance.

The general pattern of wind averaged over 6.5 years of observations showed persistent northwesterly wind over the open ocean (Fig. 6). Near the shore and over the land, the mean wind speed abruptly decreased and changed to a westerly direction. Results of the EOF analysis revealed the first three modes combined explained 60.51% of total spatial variability in wind patterns (Table 5). The first EOF mode coincided with the general direction of wind over southern California (from northwest to southeast over the ocean and from west to east over the land, Fig. 7A), and explained 32.78% of total variability. This mode was more pronounced over the ocean than over the land. The second

Table 6
Factor loadings of the first two EOF modes of rain gauge precipitation

#	Watershed	Mode 1	Mode 2
1	Santa Barbara Creek	+0.659888	−0.544046
2	Ventura River	+0.863350	−0.047230
3	Santa Clara River	+0.885640	−0.324460
4	Santa Monica Bay	+0.896001	−0.318392
5	Dominguez Channel	+0.883535	−0.306208
6	Los Angeles River	+0.938702	−0.182517
7	San Gabriel River	+0.900198	−0.003092
8	Santa Ana River	+0.937154	+0.130448
9	San Juan Creek	+0.828604	+0.069477
10	Santa Margarita River	+0.763724	+0.515268
11	San Luis Rey River/Escondido Creek	+0.728664	+0.605077
12	San Diego River	+0.802439	+0.502018

Mode 1 represents total rainstorm magnitude; Mode 2 north/south variability of rainstorms over southern California.

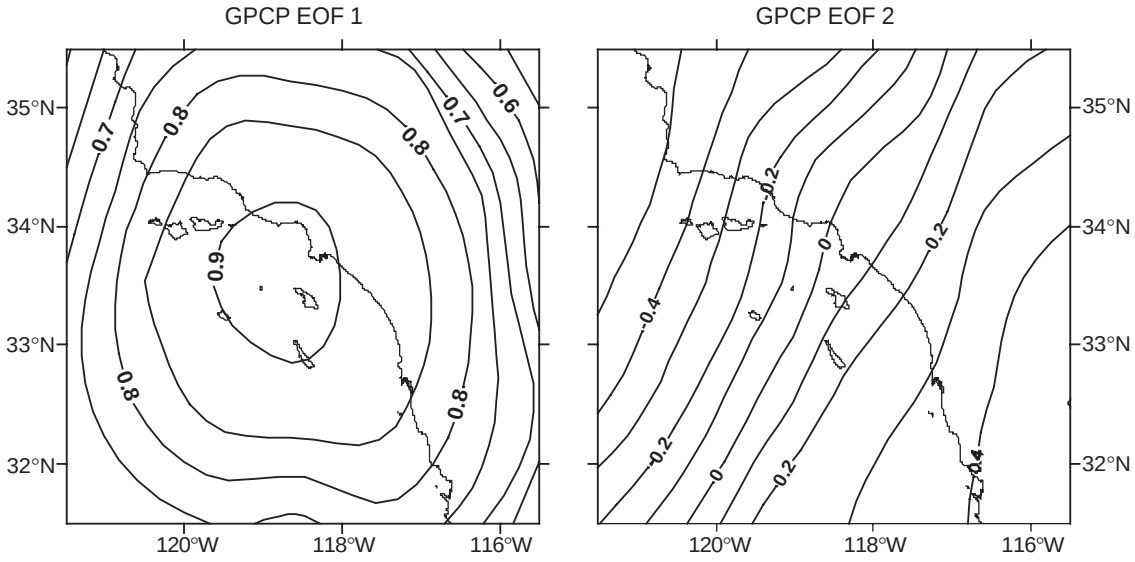

Fig. 5. Graphic representation of first and second EOF modes of remotely-sensed precipitation. The first EOF mode represents total precipitation; the second EOF mode represents the migration of the center of precipitation to the southeast.

EOF mode represented south–southwesterly wind patterns, and explained 19.56% of total spatio-temporal variability in wind patterns (Table 5). This mode was more pronounced over the land than over the ocean (Fig. 7B). The third EOF mode represented a cyclonic circulation over the Southern California Bight, called a "Catalina Eddy" (Bosart, 1983); it explained 8.17% of total variability.

Wind patterns were related to the patterns of remotely-sensed and gauge-measured precipitation, represented in the EOF modes in a similar way. To compare the inter-relationships between rainfall and wind patterns, time-lagged cross-correlation analysis was used. This analysis compared the time-series variations of the three leading EOF modes of wind and the two leading EOF modes of rain gauge-measured and remotely-sensed precipitation (Fig. 8). The first EOF mode of wind was negatively correlated with the first EOF mode of both rain gauged and remotely-sensed precipitation with time lag 1–2 days (Fig. 8A, D), meaning that a strengthening of dominating northwesterly wind results in more precipitation over the study area during the following 2 days. At the same time, the first EOF mode of wind was positively correlated with the second EOF mode of the gauge-measured precipitation with a time lag about zero, meaning that a strengthening of northwesterly wind shifts rainstorms to the southern part of the study area. The correlation between the first EOF mode of wind and the second EOF mode of

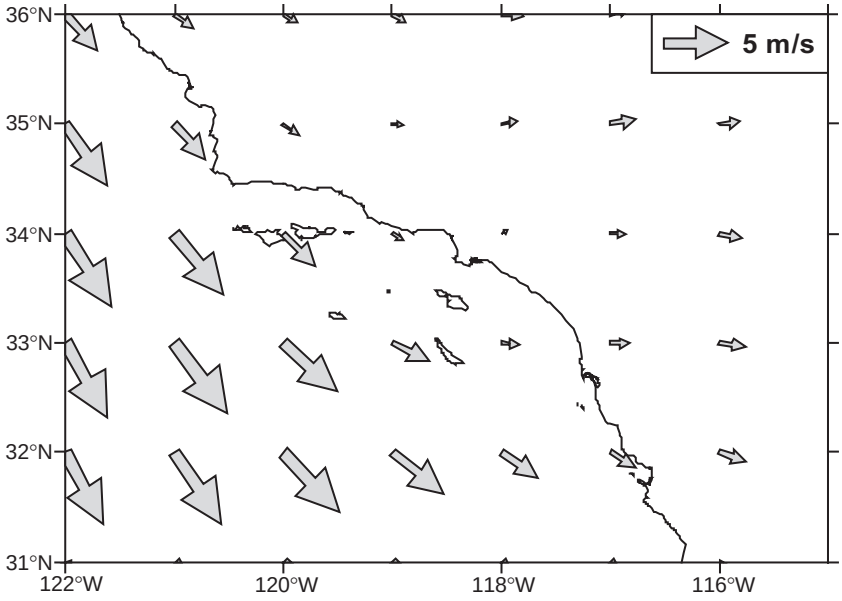

Fig. 6. Wind speed averaged over the period of March 1997–October 2003. Larger arrows indicate higher wind speed.

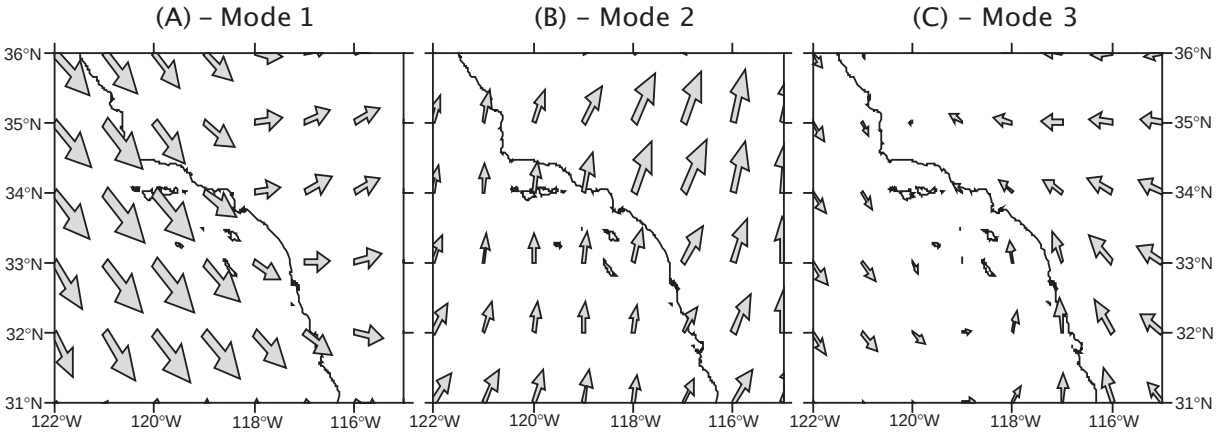

Fig. 7. Graphic representation of first (A), second (B), and third (C) EOF modes of wind speed. Larger arrows indicate higher wind speed.

remotely-sensed precipitation was similar but slightly weaker.

The second EOF mode of wind was positively correlated with the first EOF mode of the gauge-measured precipitation with a small time lag (<1 day). The correlation with the second EOF mode of the gauge-measured precipitation was small; the correlation at zero time lag was inverse and changed to positive with increase of the time lag to 1–2

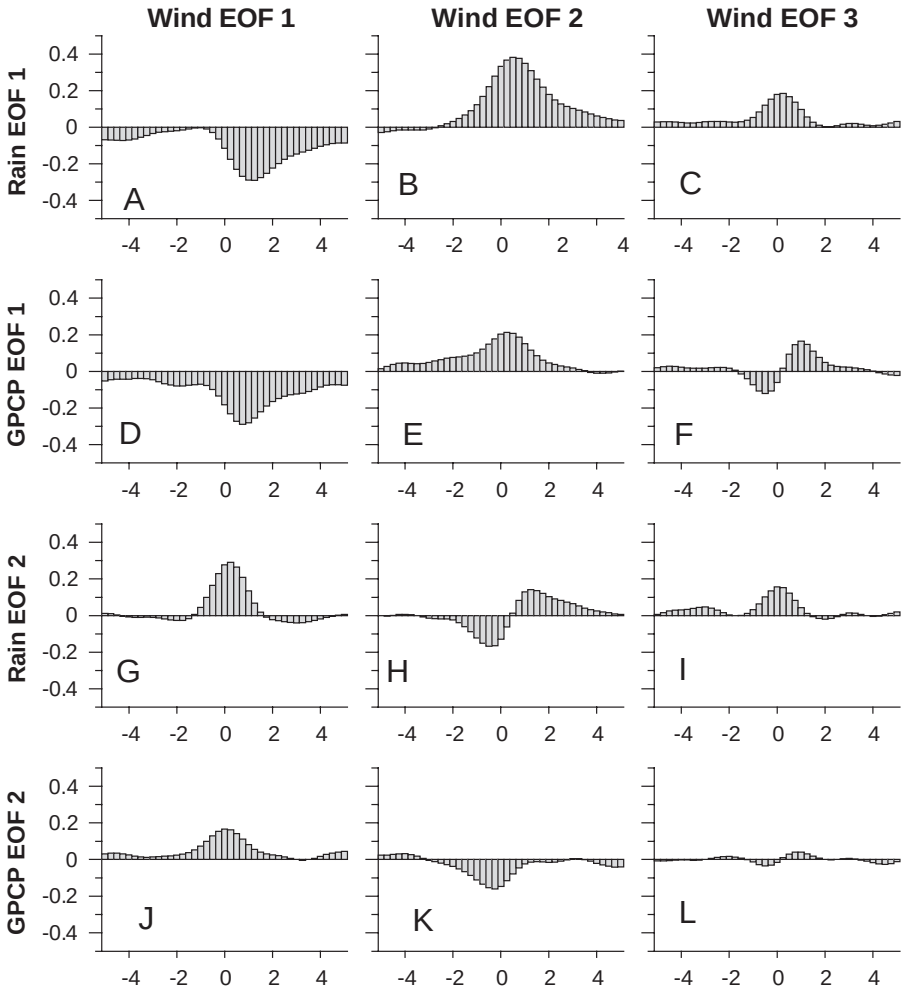

Fig. 8. Time-lagged correlations between first three EOF modes of wind and two EOF modes of the rain gauge-measured (Rain) and remotely-sensed (GPCP) precipitation. Positive time lag indicates that wind leads the precipitation.

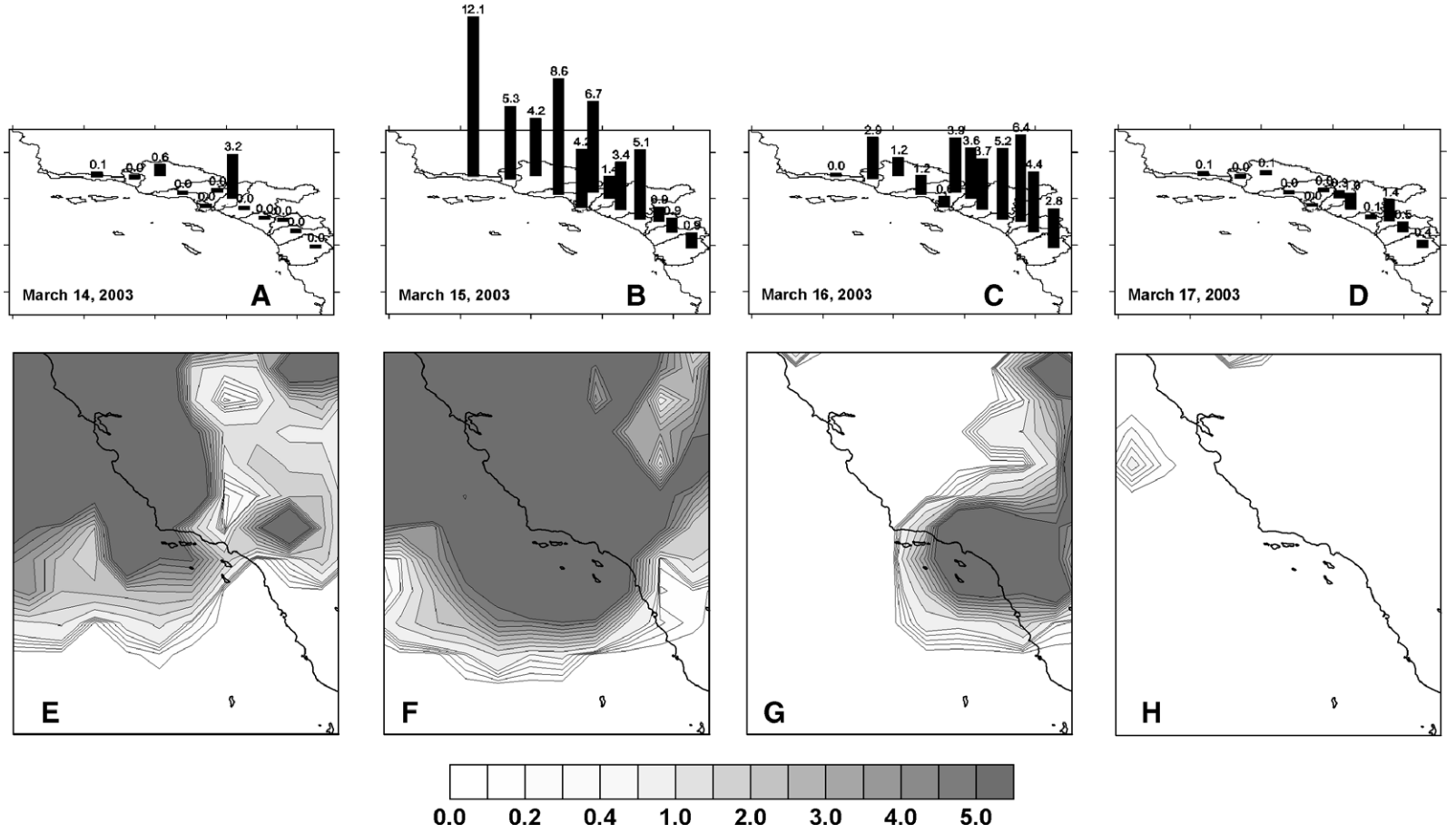

Fig. 9. Gauge-measured precipitation in southern California (A–March 14; B–March 15; C–March 16; D–March 17, 2003) and remotely-sensed precipitation in central and southern California (E–March 14; F–March 15; G–March 16; H–March 17, 2003) (cm/day).

days (Fig. 8H). These correlations indicate that strengthening of the southerly winds results in an increase of precipitation over southern California and a migration of the center of precipitation during the next 1–2 days from the south to the north. The correlations between the second EOF mode of wind and two EOF modes of the remotely-sensed precipitation were small, compared to the gauge-measured precipitation.

The correlation of the third EOF mode of wind with precipitation was small. However, the detailed analysis of the time series of the third EOF mode of wind revealed that the short periods (6–12 h) when the third wind EOF mode was extremely high (i.e., a strong cyclonic circulation over the Southern California Bight occurred) coincided with strong rainstorms.

The rainstorm observed in March 14–17, 2003 provides a typical example of the relationship between precipitation and wind patterns in southern California (Fig. 9). The rain started as a small precipitation event on March 14th and the high precipitation moved from west to east (Fig. 9A). The next day (March 15) strong rain was observed, especially in the northwestern watersheds (Fig. 9B). On March 16th the center of precipitation moved to the southeast (Fig. 9C), and on March 17th the rainfall amounts were very low (Fig. 9D). The pattern of remotely-sensed precipitation also indicated the propagation of the rainstorm from the west to the east (Fig. 9E–H). The pattern of wind circulation observed during that period (Fig. 10) showed that the beginning of the rainstorm coincided with the change of the wind direction to southwesterly on March 5th and the cyclonic eddy over the Southern California Bight on March 16th. The end of rainstorm coincided with the change of the pattern of atmospheric circulation to strong northwesterly wind.

3.3. Influence of long-term climatic cycles

In contrast to daily data, the correlation between the remotely-sensed and gauge-measured precipitation averaged annually during wet periods (July–June of the next year) was very high (Table 7). All coefficients exceeded +0.9 and were significant, in spite of very small data set ($N=7$). The correlation between the gauge-measured precipitation and the remotely-sensed precipitation in all four grid cells was higher in the southern watersheds than in the northern ones.

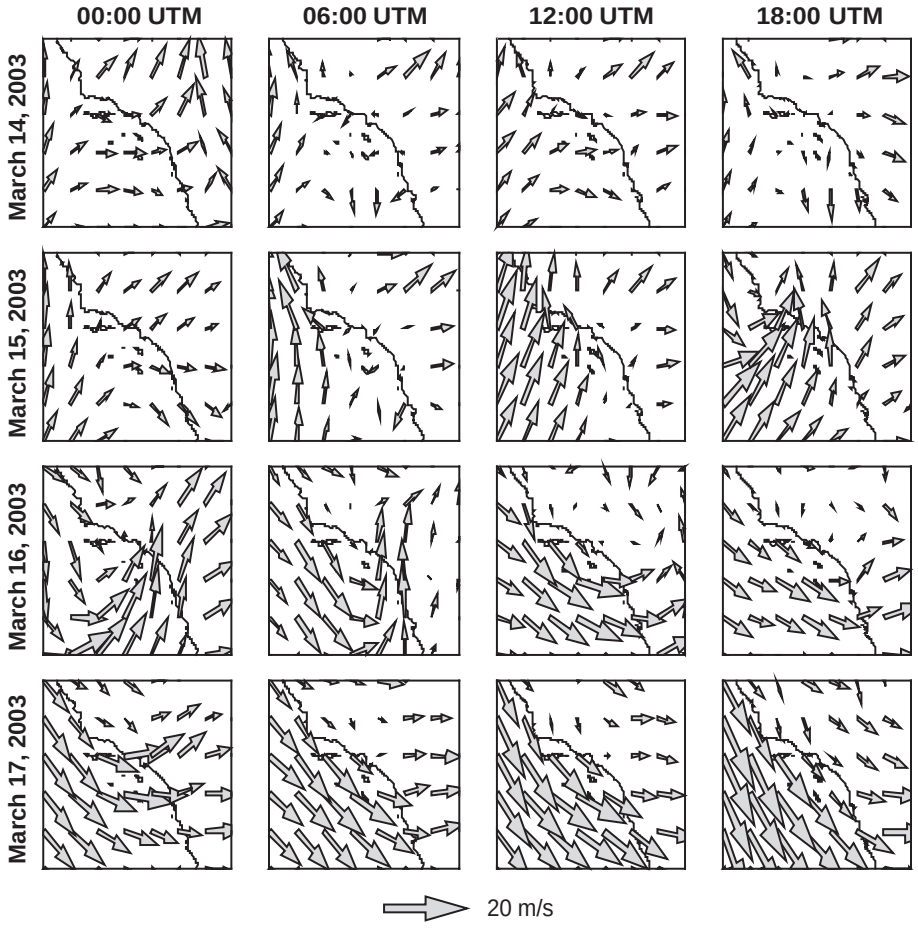

Fig. 10. Wind in southern California during the rainstorm in March 14–17, 2003.

Table 7
Correlation between annually averaged (July–June) variations of precipitation in the watersheds of southern California and the remotely-sensed precipitation in four 1° × 1° grid cells during 1996–2003

		A	B	C	D
		34°30′ N, 119°30′ W	34°30′ N, 118°30′ W	33°30′ N, 117°30′ W	32°30′ N, 116°30′ W
1	Santa Barbara Creek	+0.9615	+0.9531	+0.9522	+0.9351
2	Ventura River	+0.9836	+0.9795	+0.9691	+0.9671
3	Santa Clara River	+0.9574	+0.9722	+0.9717	+0.9720
4	Santa Monica Bay	+0.9674	+0.9783	+0.9875	+0.9525
5	Dominguez Channel	+0.9829	+0.9845	+0.9878	+0.9629
6	Los Angeles River	+0.9801	+0.9892	+0.9852	+0.9800
7	San Gabriel River	+0.9751	+0.9533	+0.9457	+0.9128
8	Santa Ana River	+0.9849	+0.9909	+0.9877	+0.9747
9	San Juan Creek	+0.9619	+0.9893	+0.9931	+0.9830
10	Santa Margarita River	+0.9552	+0.9845	+0.9763	+0.9916
11	San Luis Rey River/Escondido Creek	+0.9840	+0.9909	+0.9785	+0.9865
12	San Diego River	+0.9812	+0.9947	+0.9839	+0.9913

In spite of small number of water years ($N=7$), all correlation coefficients are significant ($p<0.05$).

Both gauge-measured and remotely-sensed monthly precipitation data were subject to long-term (i.e., intra-seasonal to interannual) variations related to global weather patterns, i.e., SOI and NINO3 indices. The first EOF modes of rain gauge-measured and remotely-sensed precipitation were almost identical (correlation +0.98, Table 8). Both modes were positively correlated with the NINO3 index (+0.28 and +0.33, respectively) and negatively correlated with the first EOF mode of wind (−0.43 and −0.46, respectively). Both time series reflect the strong El Niño event that occurred in 1997–1998, the La Niña that occurred during the second half of 1998 to early 2001, and the weak El Niño event of 2002–2003. The strong El Niño of 1997–1998 also was reflected by a strong positive NINO3 index and a strong negative SOI index during this time period (Fig. 11A, B). Maximum precipitation was observed in early 1998, during the 1997–1998 El Niño event, as indicated by strong positive values for the first EOF mode for precipitation during this time (Fig. 11C, E). Lower than normal winter season precipitation was observed in 1998–1999 and 2001–2002, corresponding with the La Niña event during this period. During these dry winter seasons, the first wind EOF mode was almost zero rather than negative as normal, indicating reduced moisture transport from the south (Fig. 11G). The negative extremes of the second EOF mode of wind during these winter seasons (1998–1999 and 2001–2002) were more persistent than normal, indicating more consistent transport of dry continental air offshore (Fig. 11H).

In contrast to the first EOF modes, the second EOF modes of remotely-sensed and gauge-measured precipitation were not correlated, and their correlation with other parameters was also different (Table 8). The second EOF mode of remotely-sensed precipitation was not correlated to the SOI and NINO3 indices, but correlated to the first EOF mode of wind (+0.34). In contrast, the second EOF mode of the gauge-measured precipitation was correlated with SOI and NINO3 indices (−0.38 and +0.30, respectively), but not correlated with the wind EOF modes. The first and second EOF modes of rain gauge-measured precipitation were positively correlated (+0.36), but the two EOF modes of remotely-sensed precipitation were not correlated.

The SOI index was correlated with the second EOF mode of rain gauge-measured precipitation (north/south variability in rain; −0.38) and the second and third EOF modes of wind (south–southwesterly and cyclonic wind patterns;

Table 8
Correlations between monthly averaged SOI and NINO3 indices and EOF modes of rain gauge-measured (Rain) and remotely-sensed (GPCP) precipitation and wind

	NINO3	Rain EOF-1	Rain EOF-2	GPCP EOF-1	GPCP EOF-2	Wind EOF-1	Wind EOF-2	Wind EOF-3
SOI	−0.77	–	−0.38	–	–	–	−0.23	+0.35
NINO3	1.00	+0.28	+0.30	+0.33	–	–	–	−0.30
Rain EOF-1	X	1.00	+0.36	+0.98	–	−0.43	–	+0.33
Rain EOF-2	X	X	1.00	+0.32	–	–	–	–
GPCP EOF-1	X	X	X	1.00	–	−0.46	–	+0.31
GPCP EOF-2	X	X	X	X	1.00	+0.34	–	–
Wind EOF-1	X	X	X	X	X	1.00	+0.34	–
Wind EOF-2	X	X	X	X	X	X	1.00	–

Only significant correlation coefficients ($p<0.05$) are given.

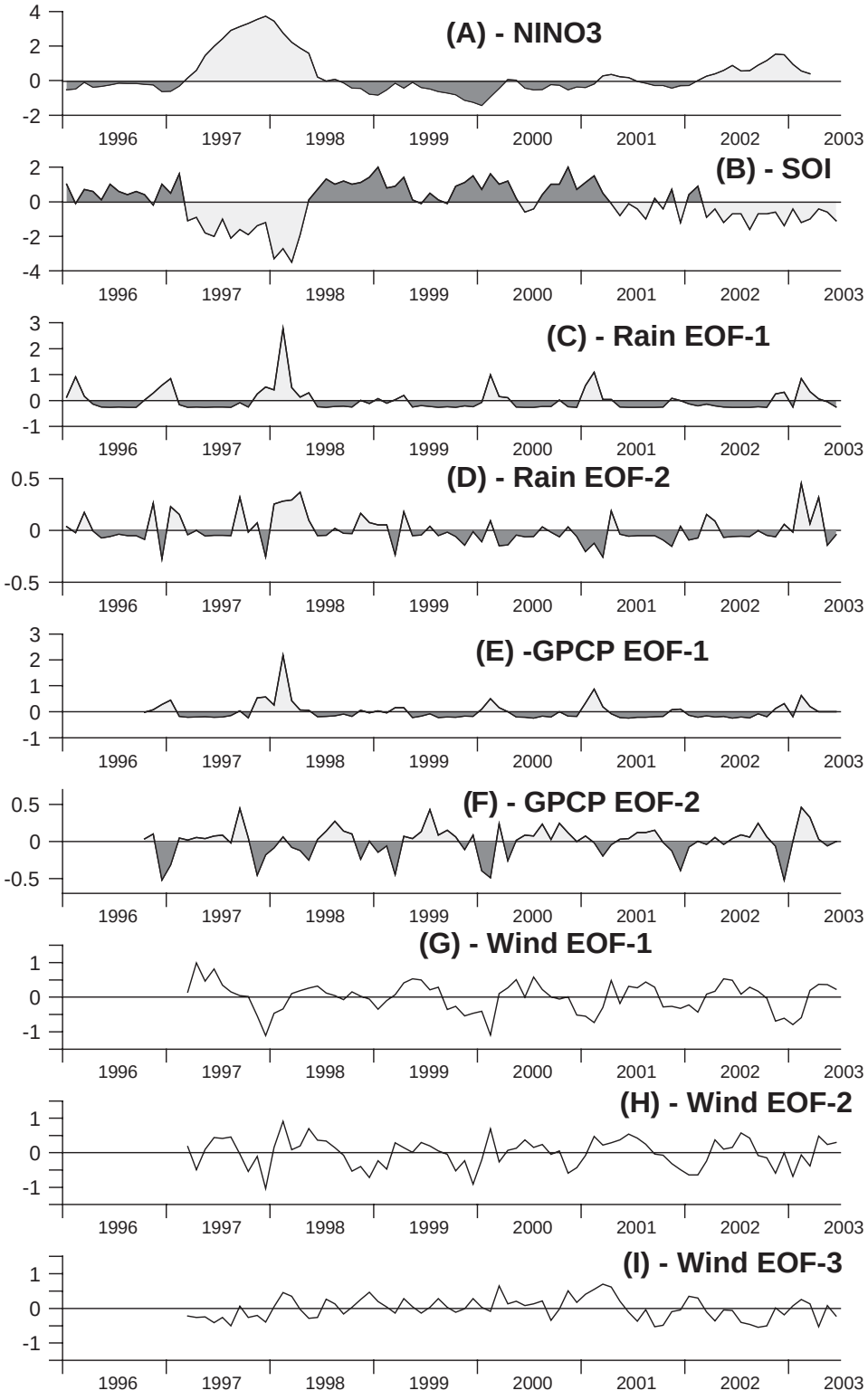

Fig. 11. Monthly averaged NINO3 (A) and SOI (B) indices; first and second EOF modes of rain gage-measured precipitation (C and D); first and second EOF modes of remote-sensed precipitation (E and F); first, second, and third leading EOF modes of wind (G, H, I).

−0.23 and +0.35, respectively). Neither the first EOF modes of wind and rain gauge-measured precipitation nor the EOF modes of remotely-sensed precipitation were correlated with the SOI index.

4. Discussion

Comparisons of remotely-sensed and gauge-measured rainfall data are inherently biased because neither method accurately

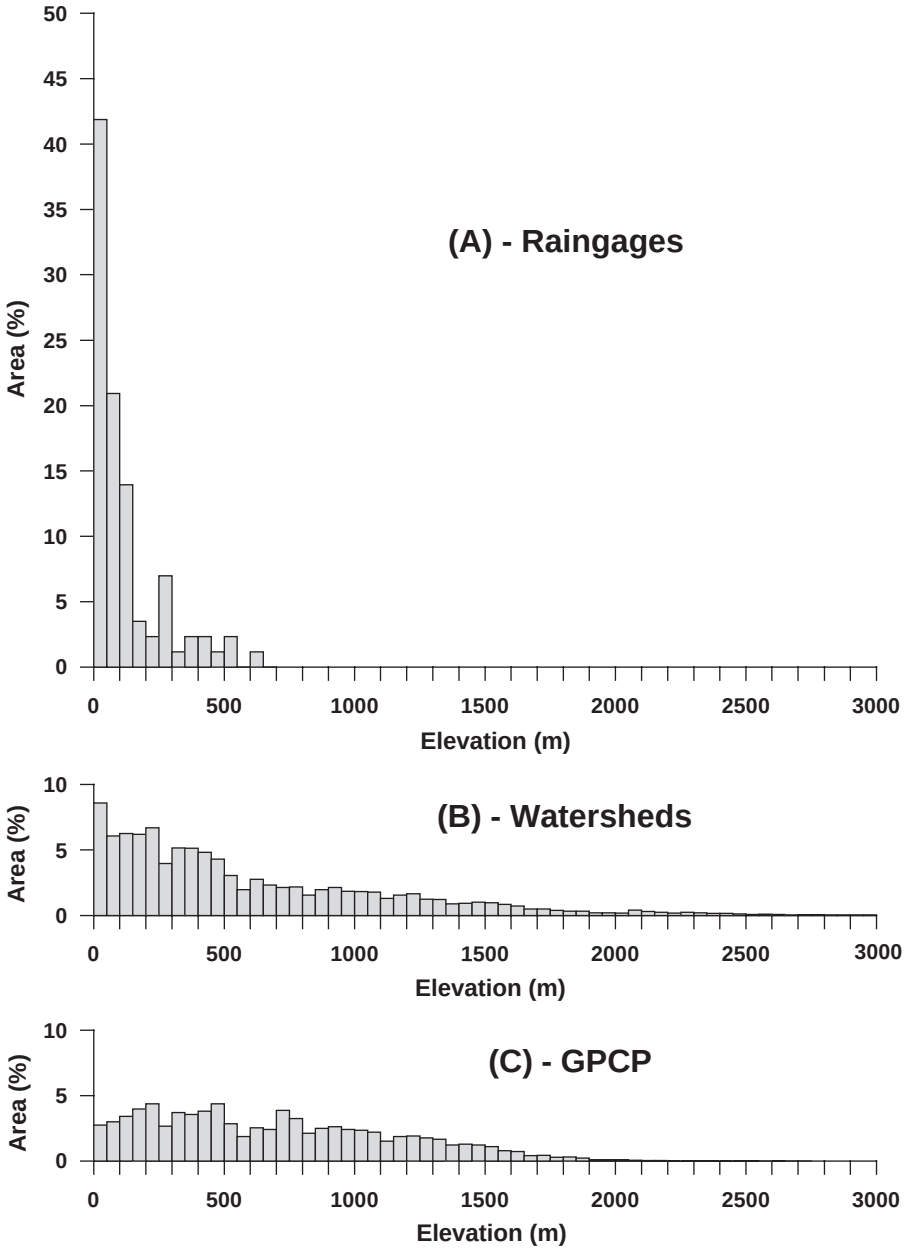

Fig. 12. Elevation of the 98 rain gauge stations (A), in all 12 watersheds (B), and in the four rectangles where remotely-sensed precipitation was measured (C).

represents the true precipitation in southern California watersheds. Orographic effects, wind patterns, and the inadequate spatial coverage of both methods contribute to their inaccuracies and to the differences between the two approaches. For example, more than 60% of rain gauge stations are located within the elevation range of 0–100 m (Fig. 12A); however, only 15% of the total area of the 12 coastal watersheds is below 100 m (Fig. 12B). Similarly, 21.6% of the total grid cell area for the remotely-sensed precipitation data is below 100 m, and 16% of that area represents sea surface (Figs. 1 and 12C). Given the increased rainfall at higher elevations (due to orographic effects), we believe that both the averaged figures of gauge-measured and especially remotely-sensed precipitation underestimate total rainfall.

Predominant westerly winds also affect the accuracy of both remotely-sensed and gauge-measured precipitation. The prevailing winds cause the coastal watersheds to experience more precipitation than inland areas. Differences in the spatial coverage of these coastal areas contribute to the differences in estimates of remotely-sensed and gauge-measured precipitation. The gauge-measured precipitation included a relatively narrow zone of the coastal watersheds (Fig. 1). In contrast, the remotely-sensed precipitation covered the entire southern California region, including vast trans-montane terrestrial areas (Figs. 2 and 5). The orientation of the mountain ranges (E–W in the northern and N–S in the southern watersheds) leads to significant variability in precipitation over southern California even during individual

storms. For example, during very strong rainstorm of February 10–12, 1992, watersheds in the northern part of the study area received much more precipitation (>300 mm) than those in the southern parts of the study area (<50 mm) (Raphael et al., 1995). The inclusion of drier inland areas in the remotely-sensed rainfall averages partly explains the consistently lower rainfall estimates than those obtained by gauge measurements.

Differences in the times of observations at different rain gauge stations can also bias comparisons based on daily observations. Observation times were different between stations and were inconsistent between storms. Considering the extreme intra-storm temporal and spatial variability of southern California rain, these differences have the potential to affect estimates of daily precipitation, especially at the beginning and the end of each rainstorm. Therefore, the synoptic comparisons we conducted may be further influenced by short-term temporal variability in rainfall between various portions of the region. We suggest that future data be collected at finer temporal scales to better describe the dynamics of individual rain events.

This study demonstrated that remotely-sensed data of atmospheric precipitation is better suited to represent general large-scale (from seasonal to interannual) regional trends and patterns of rainfall in southern California than local synoptic and spatial variability in rainfall. At the daily time-scale, the correlation between the remotely-sensed precipitation and the direct measurements of rainfall is weak (i.e., 0.3–0.5). However, the relative features of seasonal and interannual variability of precipitation can be derived from satellite observations with comparable reliability as from data measured by rain gauges. For example, at monthly and annual time scales, the correlation between the remotely-sensed and rain gauge-measured precipitation is very high (>+0.90), indicating that the rainfall observations from space are most useful for the analysis of general climatological patterns of precipitation (Arkin & Ardanuy, 1989). Finer scale analysis via remote sensing is limited by the spatial resolution of satellite data. Because satellite rainfall estimates are integrated over larger areas than rain gauge estimates, the absolute magnitudes at any particular location may be muted. Consequently, the remotely-sensed precipitation data produced at GPCP are not recommended for use where the absolute magnitude of rainfall is critical, e.g., for estimation of pollution runoff.

The difference between the behavior of the second EOF modes of remotely-sensed and gauge-measured precipitation (i.e., north–south migration of the rainstorms) is also related to the different spatial scales of these measurements. Wind patterns indicate that precipitation in southern California is generally regulated by atmospheric circulation patterns, that transport atmospheric moisture is from the south–southwest (Dorman, 1982; Dorman & Winant, 1995; Halliwell & Allen, 1987; Winant & Dorman, 1997). The variability of the second EOF mode of remotely-sensed precipitation was correlated with the first EOF mode of wind only. We speculate that over the wide area including the Southern California Bight, strengthening of the dominating northwesterly wind decreases precipitation and shifts its center to the south (the second EOF mode of remotely-sensed precipitation). The location of maximum rainfall in the coastal watersheds (the second EOF mode of the gauge-measured precipitation) did not change because the spatial scale of this zone is substantially smaller than the spatial scale of remotely-sensed precipitation data.

Low correlation between daily remotely-sensed and gauge-measured precipitation can be explained by the difference in what is actually being measured during these observations. Remotely-sensed patterns of atmospheric precipitation are based on cloud-top temperature, which is indirectly connected to precipitation, particularly on the shortest time and space scales (Huffman et al., 2001). As a result, the precipitation values in the grid cells of remotely-sensed images are often far from the physical location of gauge-measured rainfall. These differences are illustrated by the rainstorm of March 14–17, 2003 (Fig. 9). Both gauge-measured and remotely-sensed data show that the zone of precipitation propagated from the west to the east. However, both types of data exhibit high levels of spatio-temporal variability; as a result, the precipitation measured by two methods was different in each location of southern California, especially during the beginning (March 14; Fig. 9 A, E) and at the end of the rainstorm (March 17; Fig. 9 D, H).

Both first EOF modes of remotely-sensed and gauge-measured precipitation (total rainfall) were correlated with the long-term global-scale climatic NINO3 cycle. Maximum rainfall in the beginning of 1998 was attributed to the 1997–1998 El Niño event, which was the strongest of the 20th century (McPhaden, 1999). The correlation of remotely-sensed precipitation with the NINO3 index was higher than for the rain gauge-measured precipitation (Table 8); we attribute it to the fact that satellite observations measure the water vapor concentration in the atmosphere rather than the exact amount of precipitated rainfall. The warming of the surface ocean in the central equatorial Pacific (manifested in high NINO3 index) results in increased evaporation, accumulation of atmospheric moisture, and precipitation in the western USA coast, including California. At the same time, wind patterns in southern California did not change much during the El Niño period (Fig. 11 G, H).

It is important to recognize the limitations on interpreting general climatic patterns of remotely-sensed precipitation based on a relatively short period of data (8 years for this study). For example, when we compare the annual rain gauge-measured precipitation in 1996–2003 (Table 3) with long-term climatic data (Haston & Michaelsen, 1994), we see that the precipitation during the wettest year of our observations (1997/1998) was comparable or even exceeded the highest values observed during 6 centuries of reconstructed data. At the same time, the precipitation observed during the driest year (2001/2002) was also substantially higher than that of the driest years of the historical data

(Haston & Michaelsen, 1994). In contrast, the range of variability of remotely-sensed precipitation (Table 4) is within the range of historical data. The possible cause of this difference is the coarser spatial resolution of the remotely-sensed dataset. The uniformly high gauge-measured precipitation values can be explained by a "warm" PDO phase, which started in 1976–1977, when sea surface temperature in the northeastern Pacific was warmer (Mantua et al., 1997; Parrish et al., 2000) and the El Niño events were enhanced (Gershunov & Barnett, 1998). Inman and Jenkins (1999) indicate that the climate in central and southern California became wetter after 1968 (after 1977 in the watersheds to the south of San Luis Rey) and have been characterized by more frequent and extensive floods (related to ENSO) than during the previous dry period. We speculate that the increase of rainfalls in southern California was associated with the global climate shift in 1976–1977, which influenced the ecosystems all over the world (Walther et al., 2002). Whether the PDO is shifting from a warm phase back to a cold phase is currently an open question. When the 1998–1999 El Niño event changed to very strong La Niña, some scientists declared that the "warm" PDO phase is over and the "cold" phase started (Bograd & Lynn, 2003; Chavez et al., 2003; McGowan et al., 2003). To make a definite conclusion, however, we need at least a decade of future observations. Consequently, development of statistical relationships must be revisited as our understanding of long-term climate trends continues to emerge.

This study illustrates that statistical analysis of both remotely-sensed and field measured precipitation data can provide valuable insight into the mechanisms and forcing functions behind previously observed spatial and temporal patterns of wind and rainfall. These quantitative relationships provide a critical foundation for development of predictive models of relationships between climatic patterns and coastal water quality. For example, Inman and Jenkins (1999) analyzed the effect of El Niño storms on sediment flux by rivers in southern and central California and found significant relationships between climate patterns, stream flow, and sediment discharge. It is reasonable to assume that similar relationships occur for pollutants (especially those typically bound to sediments). The ability to model the effect of longer-term climatic patterns on pollutant discharge to the coast will greatly enhance management of coastal water quality. Daily remotely-sensed rainfall data produced at GPCP can be used in these studies, but is only appropriate for large-scale assessments on relative basis (e.g., interannual variability of freshwater and pollutants discharge along the entire coast of southern California). At this time, produced at GPCP remotely-sensed precipitation data is inappropriate for analysis of shorter-term or finer spatial scale patterns associated with specific storms, as well as precise quantitative estimations of rainfall. More spatially and temporally refined analyses should be based on either rain gauge-measured data or higher frequency and finer resolution remotely-sensed data, such as radar or more precise satellite imagery.

Acknowledgements

The authors thank the NASA/Goddard Space Flight Center's Laboratory for Atmospheres, which develops and computes the 1DD remotely-sensed precipitation data as a contribution to the GEWEX Global Precipitation Climatology Project. We also thank the NOAA National Data Center Climate Data Online (NNDC/CDO) for the rain gauge-measured precipitation data, the National Center for Environmental Prediction (NCEP) and the NASA Goddard Space Flight Center Distributed Active Archive Center by (GSFC DAAC) for the global wind data. We thank Stephen B. Weisberg for critical discussion of the results. Critical remarks by George Robertson and three anonymous reviewers helped to improve this paper substantially.

Appendix A

Rain gauge stations in the watersheds (WS) of southern California

WS	NCDC	WBAN	Cnt	Lat (N)	Lon (W)	H (m)	Station name
01 Santa Barbara	47902		SB	34.417	119.683	0.5	SANTA BARBARA
	47905	23190	SB	34.433	119.850	0.8	SANTA BARBARA MUNICIPAL AP
02 Ventura	46399		VE	34.467	119.250	66.0	OJAI
	49285		VE	34.283	119.300	9.7	VENTURA
03 Santa Clara	40014		LA	34.500	118.267	275.9	ACTON ESCONDIDO FC261
	42941		LA	34.700	118.433	284.3	FAIRMONT
	46161		LA	34.400	118.600	164.0	NEWHALL 5 NW
	46162		LA	34.383	118.533	115.5	NEWHALL S FC32CE
	46165		LA	34.367	118.566	130.1	NEWHALL
	47735	23187	LA	34.750	118.717	419.0	SANDBERG
	48014		LA	34.583	118.450	195.6	SAUGUS POWER PLANT 1
	49345		LA	34.483	118.133	291.2	VINCENT FS FC 120
	46569		VE	34.200	119.183	4.5	OXNARD
	46572		VE	34.217	119.133	5.8	OXNARD WSFO
	46940		VE	34.400	118.750	67.8	PIRU 2 ESE
	47957		VE	34.317	119.133	22.0	SANTA PAULA

(continued on next page)

Appendix A (*continued*)

WS	NCDC	WBAN	Cnt	Lat (N)	Lon (W)	H (m)	Station name
04 Santa Monica Bay	42214		LA	34.000	118.417	5.1	CULVER CITY
	44867		LA	34.083	118.883	148.6	LECHUZA PTRL ST FC352B
	43392		LA	34.083	118.483	102.5	GETTY CENTER
	46663		LA	33.800	118.383	20.1	PALOS VERDES EST FC43D
	47953		LA	34.000	118.500	1.3	SANTA MONI PIER
	48967		LA	34.083	118.600	69.2	TOPANGA PATROL STN FC6
	49152		LA	34.067	118.450	40.0	U C L A
05 Dominguez Channel	45114	23174	LA	33.933	118.383	9.0	LOS ANGELES INTL ARPT
	48973	3122	LA	33.800	118.333	10.2	TORRANCE MUNICIPAL ARPT
06 Los Angeles River	40144		LA	34.183	118.133	104.7	ALTADENA
	40798		LA	34.300	118.183	215.2	BIG TUJUNGA DAM FC46DE
	41194		LA	34.183	118.350	60.8	BURBANK VALLEY PUMP PLANT
	41484		LA	34.183	118.567	73.4	CANOGA PARK PIERCE COLLEGE
	42494		LA	33.933	118.150	10.2	DOWNEY FIRE STN FC107D
	44628		LA	34.217	118.250	145.4	LA CRESCENTA FC 251C
	45115	93134	LA	34.050	118.233	21.4	LOS ANGELES CVC CNTR
	45790		LA	34.017	118.100	22.3	MONTEBELLO
	46006		LA	34.233	118.067	532.6	MT WILSON NO 2
	46263		LA	34.233	118.533	79.6	NORTHRIDGE CAL STATE
	46602		LA	34.333	118.400	139.3	PACOIMA DAM FC 33 A-E
	46719		LA	34.150	118.150	80.2	PASADENA
	47785		LA	34.100	118.100	41.8	SAN GABRIEL FIRE DEPT
07 San Gabriel	42090		LA	34.100	117.883	54.2	COVINA CITY YRD FC387B
	42198		LA	34.317	117.833	498.9	CRYSTAL LAKE FC 283 C
	43452		LA	34.150	117.850	85.5	GLENDORA FC 287B
	45085	23129	LA	33.817	118.150	2.9	LONG BEACH DAUGHERTY FLD
	47050		LA	34.083	117.767	96.6	POMONA L POLY
	47749		LA	34.100	117.800	88.7	SAN DIMAS FIRE FC95
	47776		LA	34.150	117.900	69.1	SAN GABRIEL NYON P H
	47779		LA	34.200	117.867	137.6	SAN GABRIEL DAM FC425B
	49431		LA	34.000	117.867	45.3	WALNUT NI FC102C
	49660		LA	33.983	118.017	39.0	WHITTIER CITY YD FC106C
08 Santa Ana River	40192		OR	33.867	117.850	31.1	ANAHEIM
	46175	3107	OR	33.6	117.883	0.9	NEWPORT BEACH
	47888		OR	33.750	117.867	12.5	SANTA ANA FIRE STATION
	49087		OR	33.700	117.750	21.8	TUSTIN IRVINE RANCH
	49847		OR	33.883	117.817	32.5	YORBA LINDA
	40609	23156	RI	33.933	116.967	241.5	BEAUMONT 1 E
	42805		RI	33.667	117.333	119.4	ELSINORE
	47470		RI	33.950	117.383	78.0	RIVERSIDE FIRE STA 3
	47473		RI	33.967	117.367	91.6	RIVERSIDE CITRUS EXP STN
	40741		SB	34.250	116.900	628.0	BIG BEAR LAKE
	45218		SB	34.233	117.467	253.6	LYTLE CREEK R S
	47306		SB	34.050	117.183	122.4	REDLANDS
	47723		SB	34.133	117.250	105.9	SAN BERNARDINO F S 226
09 San Juan	44647		OR	33.550	117.783	3.3	LAGUNA BEACH
	47836		OR	33.533	117.550	34.8	SAN JUAN CANYON
10 Santa Margarita	46319		SD	33.383	116.800	255.5	OAK GROVE R S
	46377		SD	33.217	117.400	0.9	OCEANSIDE MARINA
	46657		SD	33.383	116.833	515.6	PALOMAR MOUNTAIN OBSERV.
	40235		RI	33.550	116.667	363.7	ANZA
11 San Luis Rey/Escondido	42863		SD	33.117	117.083	55.7	ESCONDIDO NO 2
	43914		SD	33.233	116.767	250.8	HENSHAW DAM
	49378		SD	33.233	117.233	47.4	VISTA 2 NNE
12 San Diego	40136		SD	32.833	116.767	161.2	ALPINE
	41758		SD	32.633	117.083	5.2	CHULA VISTA
	42239		SD	32.983	116.583	431.1	CUYAMACA
	42406		SD	32.850	116.617	325.2	DESCANSO RANGER STN
	42706		SD	32.817	116.983	37.6	EL CAJON
	42709		SD	32.883	116.817	55.7	EL CAPITAN DAM
	44412		SD	33.083	116.600	391.6	JULIAN CDF
	44710		SD	32.850	116.900	64.1	LAKESIDE 2 E

Appendix A (*continued*)

WS	NCDC	WBAN	Cnt	Lat (N)	Lon (W)	H (m)	Station name
12 San Diego	44735		SD	32.767	117.017	49.2	LA MESA
	47111		SD	33.017	117.033	60.2	POWAY VALLEY
	47228		SD	33.017	116.900	136.6	RAMONA FIRE DEPT
	47740	23188	SD	32.733	117.183	1.4	SAN DIEGO LINDBERGH FIELD
	47741		SD	32.767	117.233	1.4	SAN DIEGO SEAWORLD
	47874		SD	33.100	117.000	39.0	SAN PASQUAL ANIMAL PK
		93107	SD	32.867	117.133	42.6	SAN DIEGO MIRAMAR NAS
		93112	SD	32.700	117.200	4.5	SAN DIEGO NORTH ISLAND NAS

NCDC—National Climate Data Center Cooperative Station Number; WBAN—Weather Bureau, Army, and Navy Station Number; Cnt—county, Lat, Lon–station coordinates, H–elevation (m above sea level).

References

Ackerman, D., & Schiff, K. (2003). Modeling storm water mass emissions to the Southern California Bight. *Journal of Environmental Engineering*, *129*, 308–317.

Ackerman, D., & Weisberg, S. B. (2003). Relationship between rainfall and beach bacterial concentrations on Santa Monica Bay beaches. *Journal of Water and Health*, *1*, 85–89.

Ackerman, D., Schiff, K. C., & Weisberg, S. B. (2005). Evaluating HSPF in an arid, urbanized watershed. *Journal of American Water Resources Association*, *40*, N2.

Arkin, P. A., & Ardanuy, P. E. (1989). Estimating climatic-scale precipitation from space: A review. *Journal of Climate*, *2*, 1229–1238.

Bailey, H. P. (1966). *The climate of southern California*. Berkley: University of California Press. 87 pp.

Bograd, S. J., & Lynn, R. J. (2003). Long-term variability in the Southern California Current System. *Deep-Sea Research II*, *50*, 2355–2370.

Bosart, L. F. (1983). Analysis of a California Catalina eddy event. *Monthly Weather Review*, *111*, 1619–1633.

Chavez, F. P., Ryan, J., Lluch-Cota, S. E., & Niquen, M. C. (2003). From anchovies to sardines and back: Multidecadal change in the Pacific Ocean. *Science*, *299*, 217–221.

Dorman, C. E. (1982). Winds between San Diego and San Clemente Island. *Journal of Geophysical Research*, *87*, 9636–9646.

Dorman, C. E., & Winant, C. D. (1995). Buoy observations of the atmosphere along the west coast of the United States. *Journal of Geophysical Research*, *100*, 16029–16044.

Gershunov, A., & Barnett, T. P. (1998). Interdecadal modulation of ENSO teleconnections. *Bulletin of the American Meteorological Society*, *79*, 2715–2725.

Halliwell, G. R., & Allen, J. S. (1987). The large-scale coastal wind field along the west coast of North America. *Journal of Geophysical Research*, *92*, 1861–1884.

Haston, L., & Michaelsen, J. (1994). Long-term central coastal California precipitation variability and relationship to El Nico–Southern Oscillation. *Journal of Climate*, *7*, 1373–1387.

Huffman, G. J., Adler, R. F., Morrissey, M. M., Bolvin, D. T., Curtis, S., Joyce, R., et al. (2001). Global precipitation at one-degree daily resolution from multisatellite observations. *Journal of Hydrometeorology*, *2*, 36–50.

Inman, D. L., & Jenkins, S. A. (1999). Climate change and the episodicity of sediment flux of small California rivers. *Journal of Geology*, *107*, 251–270.

Lu, R., Turco, R. P., Stolzenbach, K., Friedlander, S. K., Xiong, C., Schiff, K., et al. (2003). Dry deposition of airborne trace metals on the Los Angeles Basin and adjacent coastal waters. *Journal of Geophysical Research*, *108*, 4074.

Mantua, N. J., Hare, S. R., Zhang, Y., Wallace, J. M., & Francis, R. C. (1997). A Pacific Interdecadal Climate Oscillation with impacts on salmon production. *Bulletin of the American Meteorological Society*, *78*, 1069–1079.

McGowan, J. A., Bograd, S. J., Lynn, R. J., & Miller, A. J. (2003). The biological response to the 1977 regime shift in the California Current. *Deep-Sea Research II*, *50*, 2567–2582.

McPhaden, M. J. (1999). Genesis and evolution of the 1997–98 El Nico. *Science*, *283*, 950–954.

Mount, J. F. (1995). *California rivers and streams: The conflict between fluvial process and land use*. Berkeley, CA: University of California Press. 359 pp.

Parrish, R. H., Schwing, F. B., & Mendelssohn, R. (2000). Mid-latitude wind stress: The energy source for climatic shifts in the North Pacific Ocean. *Fisheries Oceanography*, *9*, 224–238.

Priesendorfer, R. W. (1988). *Principle component analysis in meteorology and oceanography*. New York, NY: Elsevier Science. 425 pp.

Raphael, M. R., Feddema, J. J., Orme, A. J., & Orme, A. R. (1995). The unusual storms of February 1992 in southern California. *Physical Geography*, *15*, 442–464.

Tiefenthaler, L. L., & Schiff, K. C. (2003). Effects of rainfall intensity and duration on first flush of stormwater pollutants. In S. B. Weisberg, & D. Elmore (Eds.), *Southern California Coastal Water Research Project Annual Report 2001–2002* (pp. 209–215). CA: Westminster.

Vaze, J., & Chiew, F. H. S. (2003). Study of pollutant washoff from small impervious experimental plots. *Water Environment Research*, *39*, 1160–1169.

Walther, G. -R., Post, E., Convey, P., Menzel, A., Parmesan, C., Beebee, T. J. C., et al. (2002). Ecological responses to recent climate change. *Nature*, *416*, 389–395.

Ward, A. D., & Elliot, W. J. (1995). *Environmental hydrology*. Boca Raton, FL: CRC Press. 462 pp.

Winant, C. D., & Dorman, C. E. (1997). Seasonal patterns of surface wind stress and heat flux over the Southern California Bight. *Journal of Geophysical Research*, *102*, 5641–5653.